Vision-Based Control of a Handheld Surgical Micromanipulator With Virtual Fixtures

Brian C. Becker, *Member, IEEE*, Robert A. MacLachlan, *Member, IEEE*, Louis A. Lobes, Jr., Gregory D. Hager, *Fellow, IEEE*, and Cameron N. Riviere, *Senior Member, IEEE*

***Abstract*—Performing micromanipulation and delicate operations in submillimeter workspaces is difficult because of destabilizing tremor and imprecise targeting. Accurate micromanipulation is especially important for microsurgical procedures, such as vitreoretinal surgery, to maximize successful outcomes and minimize collateral damage. Robotic aid combined with filtering techniques that suppress tremor frequency bands increases performance; however, if knowledge of the operator's goals is available, virtual fixtures have been shown to further improve performance. In this paper, we derive a virtual fixture framework for active handheld micromanipulators that is based on high-bandwidth position measurements rather than forces applied to a robot handle. For applicability in surgical environments, the fixtures are generated in real time from microscope video during the procedure. Additionally, we develop motion scaling behavior around virtual fixtures as a simple and direct extension to the proposed framework. We demonstrate that virtual fixtures significantly outperform tremor cancellation algorithms on a set of synthetic tracing tasks ($p < 0.05$). In more medically relevant experiments of vein tracing and membrane peeling in eye phantoms, virtual fixtures can significantly reduce both positioning error and forces applied to tissue ($p < 0.05$).**

***Index Terms*—Dexterous manipulation, medical robots and systems, micro/nanorobots, motion control, vision-based control.**

I. Introduction

In BIOLOGY and microsurgery, proper manipulation of extremely small anatomical features often requires precision and dexterity that exceeds the capability of an unaided operator. Physiological tremor, or high-frequency involuntary hand movements with amplitudes of over 100 μm [1], is a large contributing factor to the difficulty of micromanipulation. Furthermore, lower frequency drift in gross hand positioning over time, which is caused by poor depth perception through the microscope and the relatively low bandwidth of the eye–hand feedback loop, reduces pointing accuracy [2]. Many robotic platforms have been introduced to improve manipulation during surgery, especially vitreoretinal microsurgery as extraordinarily precise micromanipulations are required to avoid sight-damaging trauma. Tiny structures commonly manipulated in the eye include veins less than 100 μm in diameter and membranes only several microns thick.

To address micromanipulation challenges in retinal surgical procedures, a variety of assistive robots have been proposed. Specific instruments such as the intraocular tool developed by Ikuta *et al*. [3] combine an actively jointed forceps with optical fiber optic illumination. Master/slave robots that are developed for eye surgery include the JPL Robot-Assisted MicroSurgery (RAMS) system [4], the Japanese occular robot of Ueta *et al*. [5], and the multiarm stabilizing micromanipulator of Wei *et al*. [6]. Retinal surgery with the da Vinci master/slave robot has been investigated [7] and led to the design of a Hexapod micropositioner accessory for the da Vinci end-effector [8]. The Johns Hopkins SteadyHand Eye Robot [9] cooperatively shares control with an operator by application of force to the robot arm holding the instrument. A unique MEMS pneumatic actuator that is called the Microhand allows grasping and manipulation of the retina [10], while the Microbots of Dogangil *et al*. aim to deliver drugs directly to the retinal vasculature via magnetic navigation [11].

Another class of micromanipulators for retinal surgery is active handheld micromanipulators, best exemplified by the Micron device [2] that is depicted in Fig. 1. Micron incorporates

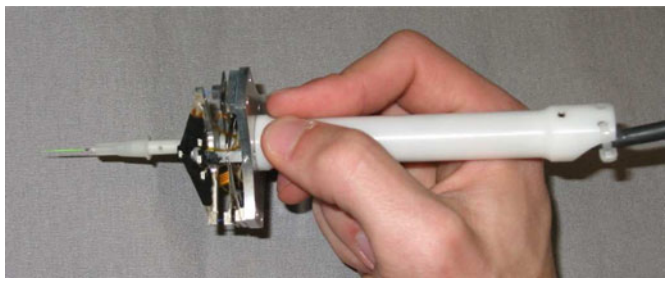

Fig. 1. Micron micromanipulator, which is shown without housing to illustrate the piezoelectric motors between the handle and tip, which enable the tip to actuate independently of the handle (or hand) motion.

Manuscript received October 31, 2012; revised December 20, 2012; accepted December 27, 2012. Date of publication February 19, 2013; date of current version June 3, 2013. This paper was recommended for publication by Associate Editor Y. Sun and Editor B. J. Nelson upon evaluation of the reviewers' comments. This work was supported in part by the National Institutes of Health under Grant R01 EB000526, Grant R21 EY016359, and Grant R01 EB007969, in part by the National Science Foundation (Graduate Research Fellowship), and in part by the Achievement Rewards for College Scientists Scholarship Foundation. This paper was presented in part at the IEEE International Conference on Robotics and Automation, Shanghai, China, May 9–13, 2011.

B. C. Becker, R. A. MacLachlan, and C. N. Riviere are with the Robotics Institute, Carnegie Mellon University, Pittsburgh, PA 15213 USA (e-mail: camr@ri.cmu.edu).

L. A. Lobes, Jr., is with the Department of Ophthalmology, University of Pittsburgh Medical Center, Pittsburgh, PA 15213 USA.

G. D. Hager is with the Department of Computer Science, Johns Hopkins University, Baltimore, Maryland 21218 USA.

This paper has supplementary downloadable material available at http://ieeexplore.ieee.org.

Color versions of one or more of the figures in this paper are available online at http://ieeexplore.ieee.org.

Digital Object Identifier 10.1109/TRO.2013.2239552

motors between the handle and the tip, effectively creating a fully active handheld tool in which the end-effector can actuate semi-independently of the hand motion within a limited range of motion (1 mm $\times$ 1 mm $\times$ 0.5 mm). Recently, we proposed a virtual fixture framework for handheld micromanipulators that integrates both tremor compensation and motion scaling [12]. This paper expands upon that work by formulation of a more general spline representation for virtual fixtures, integration of vision-based control with dense stereo vision, a new feedforward controller that is derived from [13], and extensions from planar surfaces to naturally curved surfaces. Additional evaluations, which include a vein tracing to mimic canulation and an extension of the membrane peeling experiment of [14], are explored. Furthermore, unlike previous work that presented results from novices [12]–[14], all results that are presented in this paper are completely new and performed by experienced surgeons.

Our contributions are threefold: 1) the derivation of a virtual fixture framework based on position, rather than force, control for handheld micromanipulators; 2) the integration of visual information to generate fixtures in real time that enforce task-specific behaviors for individual surgical procedures; and 3) the evaluation of the virtual fixture framework in both synthetic tracing tasks and realistic retinal procedures. Section II covers background material and introduces Micron and the system setup. Section III presents the derivation of position-based virtual fixtures for Micron. In Section IV, we test our system with medically relevant retinal experiments: synthetic task tracing, vein cannulation tracing, and membrane peeling. Finally, we conclude in Section V with a discussion of results and directions for future work.

II. Background

In general, robotic aids for surgical micromanipulation can be grouped into three categories: tremor compensation, motion scaling, and virtual fixtures. Tremor compensation is a key component of many surgical robots [2], [4], [5], [9] and aims to suppress frequency bands that are dominated by tremor in order to eliminate unwanted high-frequency motion while preserving the operator's lower frequency intended movements. In master/slave robots, tremor compensation can be achieved by insertion of various filters between the hand motion and the drive mechanism. Cooperative robots such as SteadyHand accomplish this mechanically by utilizing the inherent stiffness of the robot arm to damp high-frequency movement. Motion scaling reduces all movements; therefore, the tip only moves a set fraction of the hand movement. Scaling behavior is often used in master/slave robots [4], [5], and recent developments in handheld micromanipulation use a low-pass shelving filter [2] that acts as relative motion scaling.

Virtual fixtures, in contrast with tremor compensation or motion scaling behaviors that operate in the general case, instead improve specific motions or tasks [15]. Proposed originally by Rosenberg as a method to overlay abstract sensory information onto a force-reflecting master workspace to address latency in teleoperation [16], virtual fixtures were also found to reduce cognitive load and increase performance. In surgical operations, virtual fixtures have been used to constrain robot end-effectors to predefined areas, orientations, or behaviors for increased safety [17]–[21]. Integrating vision-based control with virtual fixtures [15] allows for more complex virtual fixtures that are constructed from anatomy [22], [23]. Most relevant to retinal surgery, Dewan *et al*. proposed virtual fixtures that were generated from dense stereo to guide the tip and orientation of the SteadyHand robot along an eye phantom retina [24], while Lin *et al*. employed virtual fixtures in a simulated retinal cannulation task [25].

In most formulations of virtual fixtures, the user manipulates a robot arm that is attached to the instrument directly or remotely via teleoperation. Forces on the robot arm are shaped and transformed to velocity commands at the instrument tip via the active virtual fixture. If the robot is nonbackdriveable, strict adherence to the virtual fixture can be enforced by ensuring that velocity components are zero in directions that move the tip away from the fixture. Unlike most virtual-fixture-enabled robots, Micron is not manipulated by the operator through the application of forces to a joystick control or robot arm. It is a fully handheld device that purely senses position; thus, the input to the virtual fixtures must be handle (or hand) motion. This fundamental difference, the use of position instead of force as the control input, necessitates the development of a unique formulation of virtual fixtures specifically designed for handheld micromanipulators.

A. Micron Manipulator

The robotic system that is used in this research is Micron, which is a previously reported 3-degree of freedom (DOF) micromanipulator [2] that has motors positioned between the handle and the instrument tip as depicted in Fig. 1. The motors are three Thunder piezoelectric actuators that are arranged in a radially symmetric pattern, which allows for tip movement independent of hand motion within a region of approximately 1 mm $\times$ 1 mm $\times$ 0.5 mm, which are centered on the handle. The operator uses Micron under a surgical microscope (Zeiss OPMI 1). A 27-gauge hypodermic needle (418-μm outer diameter) is attached to Micron, and a 127-μm nitinol wire is inserted into the needle to serve as a very fine instrument tip. The entire setup can be seen in Fig. 2.

Low-latency high-bandwidth positioning information is obtained from custom optical tracking hardware which is named ASAP [26]. Two position sensitive detectors (PSDs) act as analog cameras, tracking three LEDs on the actuated shaft of the instrument and one LED on the Micron handle. By frequency modulating at a very high rate, the 3-D positions of the LEDs can be triangulated accurately, yielding 6-DOF pose information for the Micron tip and handle. ASAP has a workspace of 4 cm^3 and measures poses at a rate of 2 kHz with errors of less than 10-μm RMS. Such high-bandwidth and accurate positioning information allows Micron to measure and control tip motion very precisely. A block diagram of the vision and control systems is shown in Fig. 3

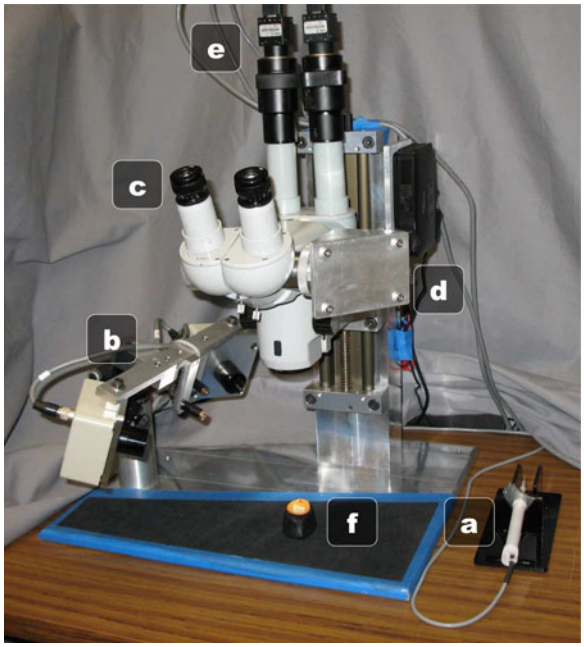

Fig. 2. System setup. (a) Micron. (b) ASAP position sensors. (c) surgical microscope. (d) Image injection system. (e) Stereo cameras. (f) Phantom half-eyeball.

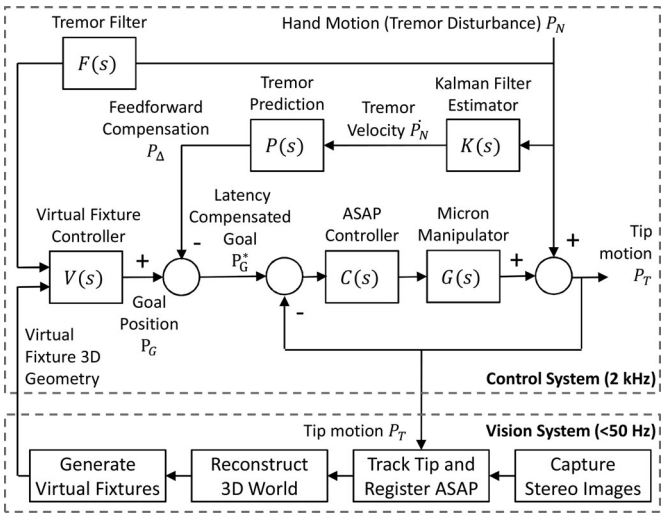

Fig. 3. Block diagram of the control and vision system. The vision system registers the cameras to ASAP and generates virtual fixture geometry from the anatomy. The control system includes feedback and feedforward paths for more precise control of the instrument tip. The virtual fixture controller uses the filtered hand motion to enforce the subspace constraints of the fixtures.

B. Control System and Notation

The tip of Micron in 3-D space is defined as $P_T \in \mathbb{R}^3$. As Micron actuates, the tip will move independently of the hand (or handle) motion; therefore, it is important to define a measure of how much the tip has moved. We define the null position as the 3-D tip position $P_N \in \mathbb{R}^3$ under the assumption that Micron is OFF, i.e., P_N exactly reflects the hand motion. One can think of P_N as being mechanically tied to the handle; thus, $P_T = P_N$ unless Micron actuates the tip. Fig. 4 graphically depicts the difference between the null position P_N and the

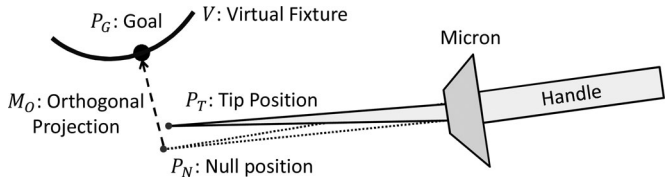

Fig. 4. Example of handheld micromanipulation with position-based virtual fixtures, which drives the tip position P_T to a goal position P_G on the virtual fixture V. The goal position is calculated by the orthogonal projection $\boldsymbol{M_O}$ of the null position P_N. The null position is the location of the tip position if the actuators were turned OFF. It is a natural selection for choosing the goal position because it is nominally the center of the actuator range of motion and exactly reflects the hand motion. (*Note:* Not to scale).

actual tip position P_T. With high-rate low-bandwidth ASAP sensors, Micron performs position-based control using closed-loop feedback with approximated linear inverse kinematics to bring the tip position P_T coincident with the goal P_G. The ASAP controller $C(s)$ in Fig. 3 uses PID for feedback control.

C. Feedforward Tremor Compensation

When a 3-D goal P_G is specified in handheld operation, typical tremor disturbance in the hand motion P_N is 90% that is rejected by a second-order low-pass Butterworth filter $F(s)$ with a corner frequency of 2 Hz. However, the remaining 10% of tremor represents 10–20 μm deviations of the tip position from the goal, making it the largest contributing factor in the error reported for hard virtual fixtures [12]. Analysis revealed that a 3-ms latency in the Micron manipulator plant $G(s)$ is largely responsible for tip positioning error [13]. We denote T as the latency between when the ASAP controller $C(s)$ sends a command to the Micron manipulator $G(s)$ and when the effect is seen in the tip position. During this time, tremor at the handle is moving the null position with a velocity $\dot{P}_N$, and to a first-order approximation, the latency in actuation introduces error P_Δ at the tip position that accumulates over time T

$$P_\Delta = \int_0^T \dot{P}_N(t)dt. \tag{1}$$

To address this latency, a feedforward control path was designed to anticipate, estimate, and compensate for the error P_Δ before it is seen by the feedback loop. As shown in Fig. 3, a constant-acceleration Kalman filter $K(s)$ is run at 2 kHz to optimally estimate the position, velocity, and acceleration states of the tip and handle. The velocity of the handle $\dot{P}_N$, which represents tremor velocity, is used by the tremor prediction module $P(s)$ to estimate tip error P_Δ that is caused by the T delay in actuation $G(s)$. Although $P(s)$ could employ a nonlinear algorithm to predict $\dot{P}_N(t)$ such as the double adaptive bandlimited multiple Fourier linear combiner [27], we found a simple predict-current-velocity at time t works well, e.g., $\dot{P}_N(t+k) = \dot{P}_N(t) \forall k \in [0, T]$. Once $P(s)$ integrates the velocity, the predicted error P_Δ is used as a feedforward term to adjust the goal position P_G to form the latency-compensated goal position P_G^*. Combined with the existing feedback control strategy, an additional 50% reduction in error is seen, for a total tremor rejection rate of 95%.

D. Vision System

Vision-based control of the manipulator is necessary because the anatomy of interest is localized via intraoperative imagery. Stereo cameras (PointGrey Flea2) attached to the microscope view the same workspace as the operator and capture up to 1024×768 resolution video at up to 50 Hz. The cameras track both the tip of the instrument and anatomical targets. However, traditional image-based visual servoing techniques [28] that operate at the low camera rates cannot provide the high bandwidth and low latencies that are needed for active control of handheld micromanipulators. Instead, the control loop must use the much faster 2-kHz ASAP positioning system. Thus, virtual fixtures are generated stereo images, which are transferred to the ASAP coordinate frame, and the resulting geometry is passed to the virtual fixture controller $V(s)$ that runs at 2 kHz in the Micron control system. The registration between the ASAP measurement system and the stereo cameras is maintained using a recursive least squares calibration procedure between the sensed tip position.

III. Position-Based Virtual Fixtures

Represented as a subspace that is defined in the 3-D Euclidean space by the stereo vision cameras, the virtual fixture V must constrain the tip position P_T of Micron, using only the hand motion of the operator P_N to guide and position the instrument tip on the virtual fixture. In the case of hard virtual fixtures, the tip of Micron should always lie on the subspace that represents the fixture; in the case of soft virtual fixtures, the error between the hand motion and the virtual fixture should be scaled. In all cases, a tremor filter $F(s)$ smoothes the tip movement. The remainder of this section devises virtual fixtures that modify the behavior of the tip P_T while using the handle motion P_N as the indicator of operator intention.

A. Point Virtual Fixture

We begin the formulation of virtual fixtures for Micron by considering the simplest fixture possible: fixing Micron's tip to a single goal point $P_G \in \mathbb{R}^3$ in space. While the point virtual fixture is active, the control system should enforce

$$P_T = P_G \tag{2}$$

regardless of where or how the operator moves the handle (within Micron's range of motion). The control from Sections II-B and II-C drives and maintains the tip at the goal position. In response to shifting anatomy, moving the virtual fixture is possible by setting a new goal point P_G. To avoid high-frequency oscillations, large changes in P_G should be smoothed with either filtration (lowpass, Kalman, etc.) or trajectory planning.

B. Higher Order Virtual Fixtures

Higher order subspaces can be built on top of the point virtual fixture to obtain more interesting behaviors. Each additional level adds a DOF to the tip motion. For instance, a line virtual fixture allows the tip to freely travel along a line while restricting motion orthogonal to the line. Likewise, we can define the hierarchy of virtual fixtures as seen in Fig. 5: point, curve, surface, and volume. It is worth considering medical relevance for each type of virtual fixture:

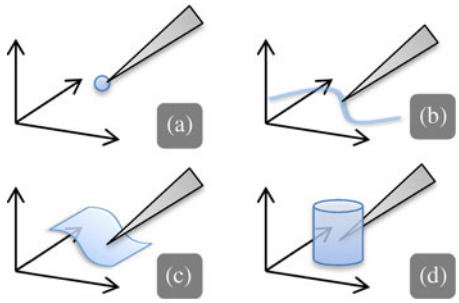

Fig. 5. Virtual fixtures constraining the tip to a subspace with increasing degrees of freedom. (a) Point. (b) Curve. (c) Surface. (d) Volume.

1) *Point* (0 DOF): steadying cannula during injection;
2) *Curve* (1 DOF): following path for laser ablation, guiding suture/needle along a blood vessel;
3) *Surface* (2 DOF): maintaining a constant standoff distance, navigating in narrow crevices;
4) *Volume* (3 DOF): restricting the tip to prevent tissue contact outside of designated "safe" volumes.

We assert that all virtual fixtures can be implemented easily with just the point virtual fixture. The key to implementing higher order fixtures with point fixtures is the selection of the correct point on the higher order virtual fixture. Geometrically, it is most intuitive to select a point on the virtual fixture as close as possible to the operator's intended position. Thus, for an arbitrary virtual fixture V, the nearest goal position P_G is the orthogonal projection of P_N onto the virtual fixture V. We define this orthogonal projection by the mapping $\boldsymbol{M_O} : \mathbb{R}^3 \rightarrow \mathbb{R}^3$ that selects the goal point P_G as the closest point from the null position P_N to the virtual fixture V

$$P_G = \boldsymbol{M_O}(V, P_N). \tag{3}$$

For simple geometric structures (lines, planes, circles, cylinders, etc.), analytic solutions for $\boldsymbol{M_O}$ exist. For more complex shapes, numerical solutions are available [30].

C. Tremor Suppression

In point virtual fixtures, all DOFs are proscribed by the fixture, eliminating unwanted tremor. However, for higher order virtual fixtures, tremor parallel to the subspace is not affected by the orthogonal projection $\boldsymbol{M_O}$. A suppression filter $\boldsymbol{F}$ between the 3-D null position P_N and the orthogonal projection $\boldsymbol{M_O}$ reduces tremor in the tip position

$$P_G = \boldsymbol{M_O}(V, \boldsymbol{F}(P_N)). \tag{4}$$

Furthermore, virtual fixtures that are generated by noisy video should be filtered as well to reduce high-frequency motions.

D. Motion Scaling

So far, we have described hard fixtures, where the tip position cannot deviate from the constraint that is imposed by the virtual

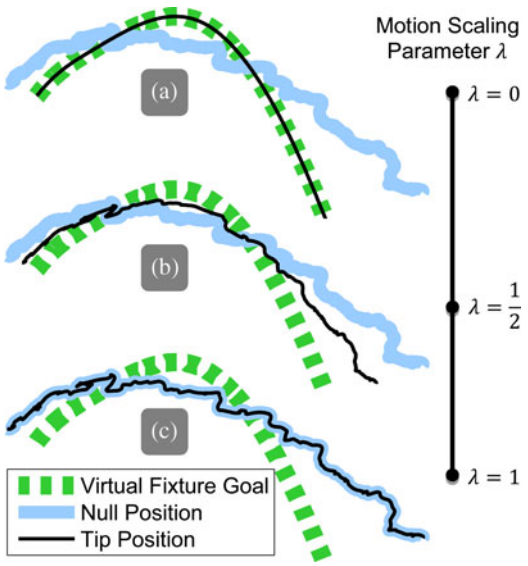

Fig. 6. Effect of motion scaling parameter λ on the tip position. (a) Hard virtual fixture (λ = 0). (b) Soft virtual fixture with λ = 1/2; control is shared 50% between virtual fixture and hand motion. (c) Fixtures off (λ = 1).

fixture. However, it is also possible to derive soft virtual fixtures that share control between the virtual fixture and the operator. An additional parameter $\lambda \in [0, 1]$ defines how much the operator can override the virtual fixture. In our formulation, λ represents the proportion of the hand motion P_N versus the goal point P_G that Micron uses to actuate the tip

$$P_T = (1 - \lambda)P_G + \lambda P_N. \tag{5}$$

In essence, λ functions as a weighted average of the goal and null position. $\lambda = 0$ corresponds to a hard virtual fixture, where the operator can only control those areas on the virtual fixture where the tip moves, while $\lambda = 1$ disables virtual fixtures entirely and leaves the operator in complete control (see Fig. 6). For values of λ between 0 and 1, the following equation can be directly manipulated into a motion scaling paradigm:

$$P_T = P_G + \lambda(P_N - P_G) \tag{6}$$

$$e = P_N - P_G \tag{7}$$

$$P_T = P_G + \lambda e. \tag{8}$$

By introducing the error e as the difference between the null position P_N controlled by the operator and the goal point P_G calculated by the virtual fixture, it is clear that the parameter λ directly represents the motion scaling factor. Thus, we can see that sharing control between the virtual fixture and the operator yields motion-scaling behavior [see Fig. 6(b)].

E. Generalizable Spline Virtual Fixtures

When applying the position-based virtual fixture framework to surgical environments, simple geometric shapes such as those that are used in our previous work [12] will not suffice; a more general fixture representation is necessary to model the complex nature of anatomical structures. A suitable representation is one of piecewise curves, or splines, which have the beneficial property of representing continuous curves and surfaces with low dimensionality and have been used with virtual fixtures [22], [24]. Additionally, the orthogonal mapping $\boldsymbol{M_O}$ can be calculated numerically for splines [29]. Fitting splines can be done directly in image space [30], or after a point-cloud representation of the anatomy of interest has been extracted. Because virtual fixtures must be available in the 3-D ASAP coordinate system, the latter approach is taken. Although a variety of spline representations may be used, we use basis-splines (B-splines) to describe general anatomy because of their versatile yet simple representation, with widespread support for fitting and evaluation. Surfaces such as the retina can be represented by a B-spline surface. Encoding a notion of "side" to the surface allows for volumetric fixtures, such as forbidding the tip to pass through the B-spline surface virtual fixture that represents the retina.

F. Generalized Position-Based Virtual Fixtures

To summarize the framework that incorporates virtual fixtures, tremor suppression, and motion scaling for handheld micromanipulators that are based on position control, the generalized control law is

$$P_G = \boldsymbol{M_O}(V, \boldsymbol{F_T}(P_N)) \tag{9}$$

$$e = \boldsymbol{F_T}(P_N) - P_G \tag{10}$$

$$P_T = P_G + \lambda e. \tag{11}$$

First, (9) selects the goal point on the virtual fixture closest to the tremor that is suppressed null position. Equation (10) then calculates the error between what the virtual fixture and where the operator is currently pointing. Finally, (11) drives the tip to either the virtual fixture or, if λ is nonzero, scales the error to achieve motion scaling about the fixture.

G. Visual Cues to Maintain Eye–Hand Coordination

A final consideration in our formulation of position-based virtual fixtures is one of practical implementation. The input to virtual fixtures is the null position, which is measured by the ASAP sensors but is otherwise unseen by the operator. Hard virtual fixtures force the tip to the fixture regardless of any hand movement, removing all error and effectively disrupting the eye–hand coordination feedback loop. With the eye–hand feedback loop broken, the operator will unknowingly drift away from the virtual fixture until the virtual fixture is no longer within Micron's range of motion. At this point, active control becomes impossible because the motors have saturated. Thus, it is imperative to provide a surrogate sense of error to restore eye–hand coordination.

In order to prevent this unbounded drifting behavior, we display visual cues that indicate the 3-D location of the unseen null position. As shown in Fig. 7, we choose visual cues in the form of two circles: a green one to show the goal location and a blue one to show the null position, which reflects the actual hand movements. The distance between the circle centers represents the error that Micron is currently eliminating. Z error is displayed by varying the radius of the null position circle, e.g., a growing radius represents upward drift. The operator is

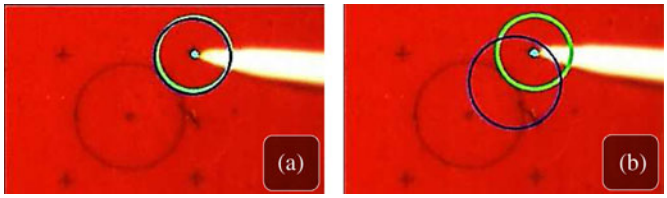

Fig. 7. Micron enforcing a point hard virtual fixture with visual cues: green represents the goal, blue represents the null position. (a) Nearly coincident circles are desirable, indicating Micron is near the center of the range of motion. (b) Position and size of the blue circle indicates drift. Here, the operator has drifted left, down, and upward in the X, Y, and Z directions, respectively. If Micron was turned OFF, the tip would snap to the blue circle.

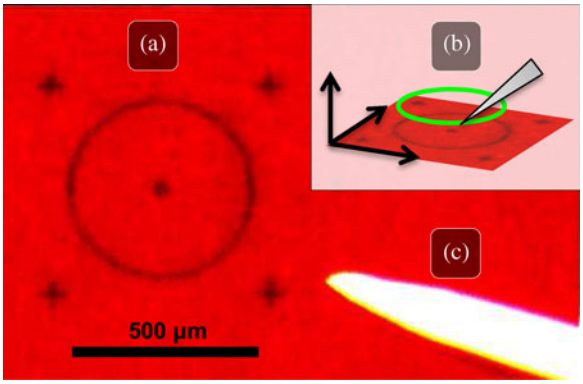

Fig. 8. (a) Laser etched target onto rubber surface. (b) Generating a 3-D circle virtual fixture from the tracked target. (c) White-painted, tapered tip of Micron.

instructed to keep the two circles roughly coincident to prevent drifting and saturation of the motors.

IV. Evaluation

In order to assess the performance of the proposed virtual fixture framework in surgically relevant situations, three experiments were performed in phantoms: basic synthetic tracing, vein cannulation tracing, and retinal membrane peeling. While previously reported results from [2], [12] only used novices with no surgical experience, all results that are presented here are newly performed with trained surgeons.

A. Synthetic Tracing Above Rubber Slide

Similar to [2], we performed simple synthetic tracing tasks above a rubber slide to assess general micromanipulation performance in unaided cases, with general tremor compensation, and with hard and soft virtual fixtures. As shown in Fig. 8, the rubber slide had a laser-etched target that consists of four crosses arranged as the corners of a 600 μm square, with a circle of 500 μm diameter in the middle. Three tasks were performed at 29$\times$ magnification (see Fig. 8).

1) *Hold still:* Hold the tip of the instrument 500 μm above a fiducial on a plane for 30 s. A point fixture that is located above the top right cross was used.
2) *Circle tracing:* Trace a circle with a 500 μm offset from rubber surface two times. A 3-D circle fixture that is derived from the tracked rubber target was used.
3) *Move and hold:* Move between the four corners of a square sequentially, pausing at each corner. Four plane segments that are oriented vertically and connecting each of the four corners were used, forming a compound box fixture.

To construct the virtual fixtures for each case, hierarchical template matching is used to locate the target. Once the target is located in both images, the center of the target can be backprojected into 3-D using the camera registration. Individual virtual fixtures (point, circle, box) are derived from the 3-D location of the target and the relative distances of the components. All tracking and virtual fixture generations happen at 50 Hz with a custom resolution of 504 $\times$ 324.

For each task, four different scenarios were performed by three trained surgeons in random order.

1) *Unaided*: Micron was turned OFF.
2) *Aided with the shelving filter*: Micron was turned ON with the tremor suppressing shelving filter from [2].
3) *Aided with soft virtual fixtures*: Micron was turned ON using virtual fixtures with the motion scaling factor $\lambda = 1/5$; therefore, errors were reduced by 5$\times$.
4) *Aided with hard virtual fixtures*: Micron was turned ON with virtual fixtures but no motion scaling ($\lambda = 0$).

Each set of synthetic experiments on the rubber slide was performed by three surgeons at least once, for a total of seven sets and 84 trials. Visual cues were displayed on a 3-D monitor. All error was measured at 2 kHz as the Euclidean distance between the tip position sensed by the ASAP optical trackers and the closest point on the virtual fixture.

B. Vein Cannulation Tracing in Eyeball Phantom

To evaluate the virtual fixture framework beyond the simple tasks of previously reported work [12] and to simulate a more realistic task in a more relevant surgical environment than a rubber slide, we present a new task simulating vein cannulation in which drugs need to be injected into tiny retinal vessels. An eye phantom with a curved vein was constructed on the bottom half of a 42-mm diameter sphere; the curved "vein" was a red-painted hair taped on a yellow paper background that was firmly glued to the inside of a ping-pong ball (see Fig. 9). Under 11$\times$ magnification, the surgeon was asked to follow a 10-mm segment of a curved vein on the inside of a sphere, maintaining a 500-μm vertical distance from the spherical surface. The same four scenarios as the synthetic tracing experiments were performed by a single vitreoretinal surgeon for a total of seven sets (28 trials).

The vision system for the vein tracing experiment uses higher 1024 $\times$ 768 resolution stereo images that are captured at 30 Hz to perform a dense 3-D reconstruction using the fast semiglobal block matching (SGBM) algorithm [31]. The vein is localized with color trackers, filtered with blob analysis, skeletonized with morphological and distance transforms, and is fit to a B-spline in the *XY* image space and *XZ* direction that are based on the disparity map. The B-spline is then backprojected to form a full 3-D representation of the vein on the surface (see Fig. 9). Because the anatomy of greatest interest is often occluded by the tip, partially observed splines are matched with iterative closet

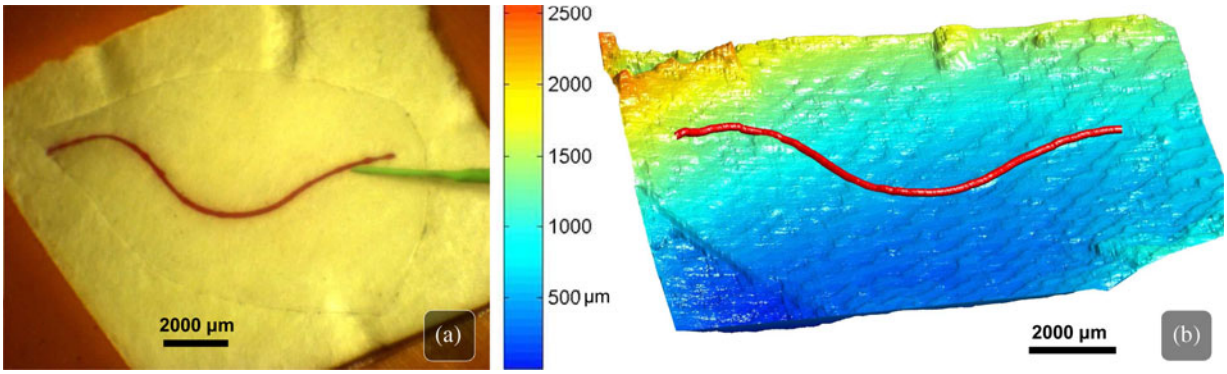

Fig. 9. (a) Half-eyeball phantom with a dyed hair tapped to yellow paper affixed to the inside of a ping-pong ball with green-painted tip of Micron visible. (b) 3-D reconstruction and 3-D spline representation of the vein, with dark blue representing low s positions and dark orange representing high Z positions. Although the vein lies on the surface, it is visualized with red; additionally, the vein is represented as a tube for illustration, in reality it is much flatter.

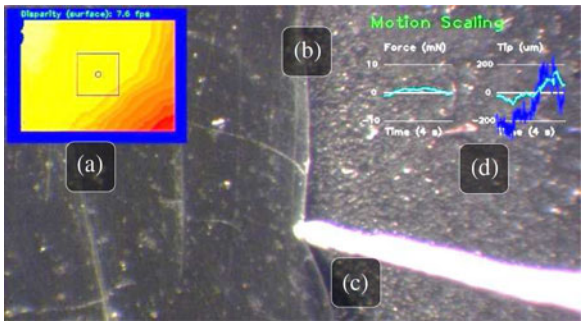

Fig. 10. Retinal membrane peeling on sorbothane slide. (a) Disparity map. (b) Edge of the 12-μm plastic wrap. (c) Tip of Micron peeling the plastic wrap "membrane." (d) Force and displacement graphs for visualization.

point (ICP) [32] to the initial unoccluded spline and occluded sections are filled in with linear interpolation. Full disparity maps and 3-D spline representations are updated at 2 Hz and provided to the virtual fixture controller.

C. Retinal Membrane Peeling With Plastic Wrap Phantom

For evaluation of the virtual fixtures in contact with tissue, we use our framework in the task of retinal membrane peeling, a challenging microsurgical task that requires extremely delicate micromanipulation to engage and peel 5-μm-thick membranes off the retina. In contrast with [2], which used rubber as a phantom retina, we use a sorbothane slide to better mimic retinal tissue deformation and place 12-μm plastic wrap on top to simulate the task of peeling. Dense stereo reconstructs 640 $\times$ 480 resolution disparity maps at 10 Hz; a local plane is fit around the tip of Micron to measure Z displacement from the surface (see Fig. 10).

Unlike the previous tracing tasks that focus on positioning, the goal of the peeling experiment is to minimize forces that are applied to the simulated retinal tissue. A force sensor below the sorbothane slide measured both downward and upward directions at 2 kHz. However, force information is only used for evaluation. All control of Micron is vision based using Z displacement that is measured by the stereo cameras. During the procedure, tremor suppression and velocity limits smooth tremor while peeling. A volumetric soft virtual fixture that extends from 50 μm above the surface to 50 μm below the surface scales motions in the Z direction with $\lambda = 1/3$ to increase precision during the engagement of the membrane. Based on distance to force proportionality and device limits, a hard stop was chosen at 50 μm below the surface to prevent excessive downward force. Visual cues indicate when hard stops are reached. An experienced vitreoretinal surgeon performed 20 unaided and aided trials total in a random order.

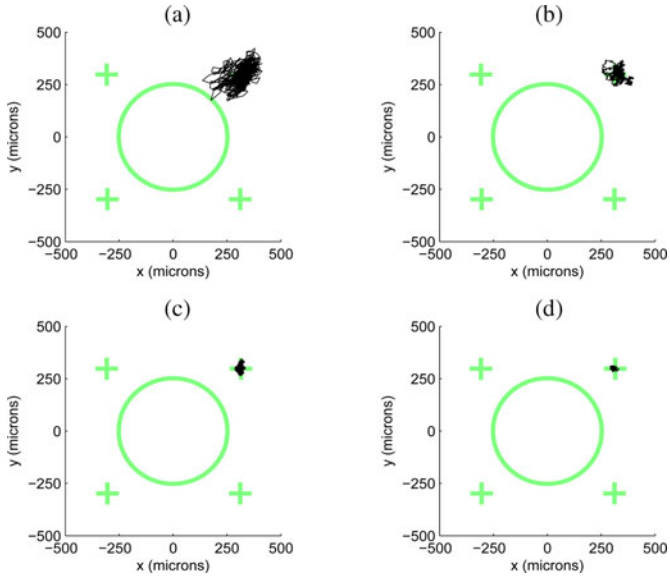

Fig. 11. Hold still results (a) unaided (b) aided with shelving filter (c) aided with soft fixtures (d) aided with hard fixtures.

D. Results

For each of the experiments, trained surgeons performed the trials, and statistical significance was assessed with a two-tailed t-test. For tracing tasks, Figs. 11–14 show representative trace histories of the tip locations in black for each task and scenario on the target represented by thick light green lines. Quantitatively, Fig. 15(a) presents mean 3-D RMS error for all tracing tasks and Table I shows max error. It is important to note that the vein tracing task has a higher incident of saturation and thus more error because of the lower magnification and the

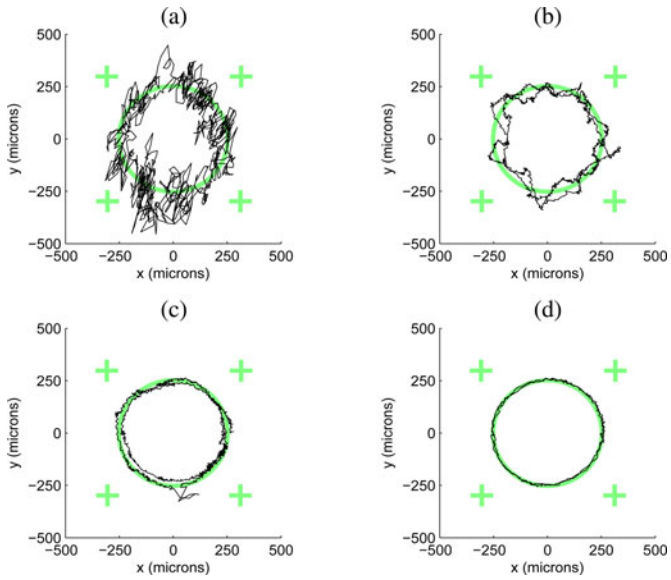

Fig. 12. Circle tracing results. (a) Unaided. (b) Aided with shelving filter. (c) Aided with soft fixtures. (d) Aided with hard fixtures.

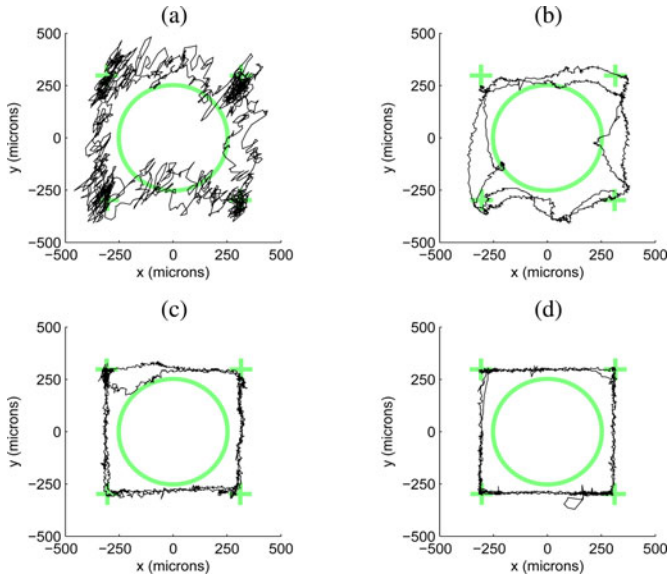

Fig. 13. Move and hold results. (a) Unaided (b) Aided with shelving filter. (c) Aided with soft fixtures. (d) Aided with hard fixtures. Deviations from the virtual fixtures in (c) and (d) result from saturation of the actuators, caused by tremor or drift in excess of the range of motion of Micron.

TABLE I
MAX ERROR IN POSITIONING TASKS

Task	Unaided	Aided		
	Micron Off (μm)	Shelving Filter (μm)	Soft Fixtures (μm)	Hard Fixtures (μm)
Hold Still	**480±214**	**261±99**	99± 40	87±41
Circle Tracing	**710±500**	**711±262**	302±260	105±72
Move/Hold	**326±501**	**305±167**	132±96	126±43
Vein Tracing	**701±177**	492±121	415±226	383±177

Mean of the 3D max error across all seven trials of each combination of task and scenario. Significantly reduced results compared to the hard fixtures case are bolded ($p < 0.05$). Because vein tracing experiments used lower magnification and larger motions were necessary (10 mm), saturation was encountered more frequently than in other tasks.

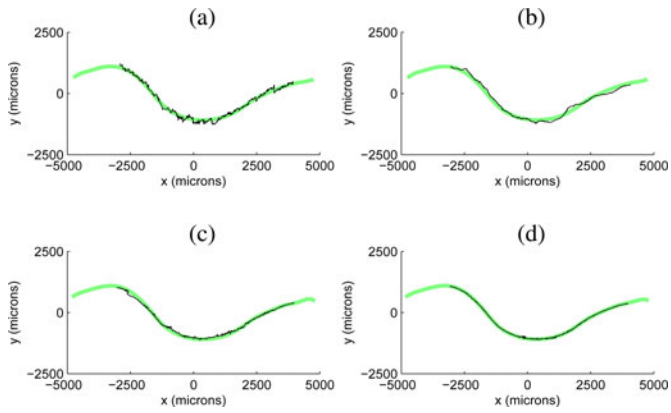

Fig. 14. Vein tracing results. (a) Unaided. (b) Aided with shelving filter. (c) Aided with soft fixtures. (d) Aided with hard fixtures.

greater tip traversal required (almost 10 mm, compared with the 0.5-mm circle). In fact, 98% of the error during the vein tracing task with hard virtual fixtures occurs while the manipulator is in saturation.

In all cases, mean RMS error and maximum error for hard virtual fixtures are significantly less than in the unaided case for 3-D measurements ($p < 0.05$). Mean error of hard virtual fixtures for 3-D is significantly less than the state-of-the-art shelving filter from [2] ($p < 0.05$). Fig. 15(b) shows the average maximum upward and downward forces that are measured during the peeling experiments. Vision-based virtual fixtures significantly reduce forces, and downward forces are greatly reduced by the hard-stop virtual fixture ($p < 0.05$).

V. DISCUSSION AND CONCLUSION

In this paper, we have presented a derivation of virtual fixtures that depends not on forces that are applied to a robot arm, but on the motion of the handle of the instrument. This new position-based virtual fixture formulation is necessary for the class of handheld micromanipulators, such as Micron, that use handle positions as input to the control system. Virtual fixtures are generated in real time from stereo cameras that are attached to the microscope, providing task-dependent behaviors to the operator. Visual cues are displayed to the operator to maintain eye–hand coordination and help guide the operator.

Hard virtual fixtures totally constrain the tip, enforcing constraints that should never be violated, e.g., forbidden areas or snap-to behaviors. Implementation of soft virtual fixtures under our formulation directly results in intuitive motion scaling. In all cases, tremor suppression filters compensate for unwanted high-frequency motion. Furthermore, the virtual fixture framework easily adapts to general parameterizations such as splines to model complex anatomy. Using Micron as a test platform, virtual fixtures have been validated with medically relevant artificial tests, such as vein tracing to significantly reduce tip positioning error. In retinal membrane peeling with tissue contact, virtual fixtures can significantly reduce forces using only visual information.

A new 6-DOF Micron prototype with a larger range of motion should reduce saturation and improve performance. Future work

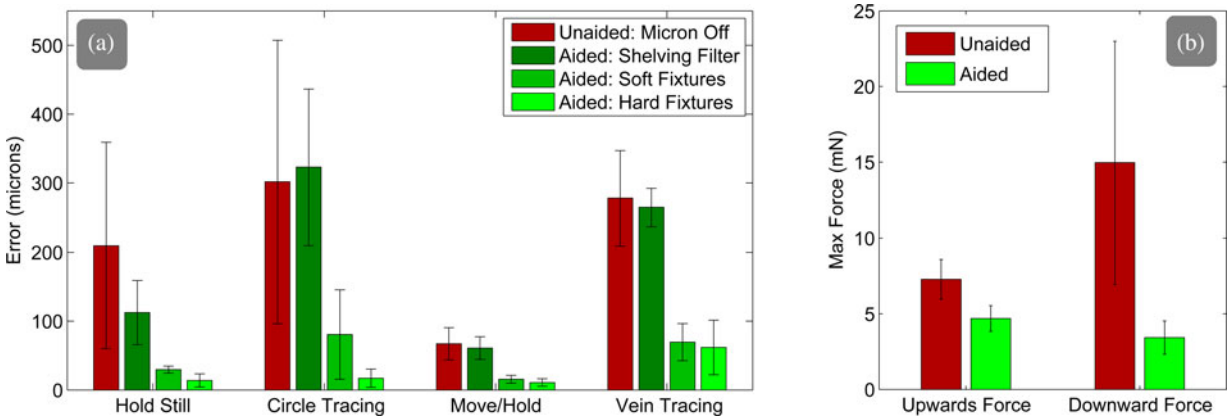

Fig. 15. (a) Mean 3-D RMS error across seven trials of each combination of task and scenario, with standard deviation error bars. Hard fixtures significantly reduce error compared with unaided and shelving filter scenarios ($p < 0.05$). (b) Maximum upward and downward force per trial, averaged over ten randomized unaided and aided runs each. Virtual fixtures significantly reduce both upward and downward forces ($p < 0.05$).

includes orientation-based virtual fixtures to enforce a remote center of motion at the port to minimize eye motion or perform laser therapies. Testing in more realistic situations *in vivo* is needed in order to fully validate efficacy in retinal surgery and determine optimal scaling parameters.

REFERENCES

[1] S. P. N. Singh and C. N. Riviere, "Physiological tremor amplitude during retinal microsurgery," in *Proc. IEEE Northeast Bioeng. Conf.*, 2002, pp. 171–172.

[2] R. A. MacLachlan, B. C. Becker, J. Cuevas Tabares, G. W. Podnar, L. A. Lobes, Jr., and C. N. Riviere, "Micron: An actively stabilized handheld tool for microsurgery," *IEEE Trans. Robot.*, vol. 28, no. 1, pp. 195–212, Feb. 2012.

[3] K. Ikuta, T. Kato, and S. Nagata, "Micro active forceps with optical fiber scope for intra-ocular microsurgery," *IEEE Micro. Electro. Mech. Syst.*, pp. 456–461, Feb. 1996.

[4] H. Das, H. Zak, J. Johnson, J. Crouch, and D. Frambach, "Evaluation of a telerobotic system to assist surgeons in microsurgery," *Comput. Aided Surgery*, vol. 4, no. 1, pp. 15–25, 1999.

[5] T. Ueta, Y. Yamaguchi, Y. Shirakawa, T. Nakano, R. Ideta, Y. Noda, A. Morita, R. Mochizuki, N. Sugita, and M. Mitsuishi, "Robot-assisted vitreoretinal surgery: Development of a prototype and feasibility studies in an animal model," *Ophthalmology*, vol. 116, no. 8, pp. 1538–1543, 2009.

[6] W. Wei, R. E. Goldman, H. F. Fine, S. Chang, and N. Simaan, "Performance evaluation for multi-arm manipulation of hollow suspended organs," *IEEE Trans. Robot.*, vol. 25, no. 1, pp. 147–157, Feb. 2009.

[7] D. H. Bourla, J. P. Hubschman, M. Culjat, A. Tsirbas, A. Gupta, and S. D. Schwartz, "Feasibility study of intraocular robotic surgery with the da Vinci surgical system," *Retina*, vol. 28, no. 1, pp. 154–158, 2008.

[8] A. P. Mulgaonkar, J. P. Hubschman, J. L. Bourges, B. L. Jordan, C. Cham, J. T. Wilson, T. C. Tsao, and M. O. Culjat, "A prototype surgical manipulator for robotic intraocular micro surgery," *Stud. Health Technol. Inform.*, vol. 142, no. 1, pp. 215–217, 2009.

[9] A. Uneri, M. A. Balicki, J. Handa, P. Gehlbach, R. H. Taylor, and I. Iordachita, "New steady-hand eye robot with micro-force sensing for vitreoretinal surgery," in *Proc. IEEE Int. Conf. Biomed. Robot. Biomechatron.*, Sep. 2010, pp. 814–819.

[10] J. P. Hubschman, J. L. Bourges, W. Choi, A. Mozayan, A. Tsirbas, C. J. Kim, and S. D. Schwartz, "The microhand: A new concept of micro-forceps for ocular robotic surgery," *Eye*, vol. 24, no. 2, pp. 364–367, 2009.

[11] G. Dogangil, O. Ergeneman, J. J. Abbott, S. Pané, H. Hall, S. Muntwyler, and B. J. Nelson, "Toward targeted retinal drug delivery with wireless magnetic microrobots," in *Proc. IEEE Intl. Conf. Intell. Robot. Syst.*, Sep. 2008, pp. 1921–1926.

[12] B. C. Becker, R. A. MacLachlan, G. D. Hager, and C. N. Riviere, "Handheld micromanipulation with vision-based virtual fixtures," in *Proc. IEEE Int. Conf. Robot. Autom.*, May 2011, pp. 4127–4132.

[13] B. C. Becker, R. A. MacLachlan, and C. N. Riviere, "State estimation and feedforward tremor suppression for a handheld micromanipulator with a Kalman filter," in *Proc. IEEE Intl. Conf. Intell. Robot. Syst.*, Sep. 2011, pp. 5160–5165.

[14] B. C. Becker, R. A. Maclachlan, L. A. Lobes, Jr., and C. N. Riviere, "Vision-based retinal membrane peeling with a handheld robot," in *Proc. IEEE Int. Conf. Robot. Autom.*, May 2012, pp. 1075–1080.

[15] A. Bettini, P. Marayong, S. Lang, A. M. Okamura, and G. D. Hager, "Vision-assisted control for manipulation using virtual fixtures," *IEEE Trans. Robot.*, vol. 20, no. 6, pp. 953–966, Dec. 2004.

[16] L. B. Rosenberg, "Virtual fixtures: Perceptual tools for telerobotic manipulation," in *Proc. IEEE Virt. Reality Annu. Intl. Symp.*, Sep. 1993, pp. 76–82.

[17] J. Funda, R. H. Taylor, B. Eldridge, S. Gomory, and K. G. Gruben, "Constrained Cartesian motion control for teleoperated surgical robots," *IEEE Trans. Robot. Autom.*, vol. 12, no. 3, pp. 453–465, Jun. 1996.

[18] B. L. Davies, S. J. Harris, W. J. Lin, R. D. Hibberd, R. Middleton, and J. C. Cobb, "Active compliance in robotic surgery—The use of force control as a dynamic constraint," *Proc. Inst. Mech. Eng., H: J. Eng. Med.*, vol. 211, no. 4, pp. 285–292, 1997.

[19] S. Park, R. Howe, and D. Torchiana, "Virtual fixtures for robotic cardiac surgery," in *Proc. Med. Image Comput. Comput. Assist. Interv.*, 2001, pp. 1419–1420.

[20] C. A. Moore, Jr, M. A. Peshkin, and J. E. Colgate, "Cobot implementation of virtual paths and 3D virtual surfaces," *IEEE Trans Robot. Autom.*, vol. 19, no. 2, pp. 347–351, Apr. 2003.

[21] A. Kapoor, M. Li, and R. H. Taylor, "Constrained control for surgical assistant robots," in *Proc. IEEE Int. Conf. Robot. Autom.*, May 2006, pp. 231–236.

[22] M. Li, M. Ishii, and R. H. Taylor, "Spatial motion constraints using virtual fixtures generated by anatomy," *IEEE Trans. Robot.*, vol. 23, no. 1, pp. 4–19, Feb. 2007.

[23] J. Ren, R. V. Patel, K. A. McIsaac, G. Guiraudon, and T. M. Peters, "Dynamic 3-D virtual fixtures for minimally invasive beating heart procedures," *IEEE Trans. Med. Imag.*, vol. 27, no. 8, pp. 1061–1070, Aug. 2008.

[24] M. Dewan, P. Marayong, A. M. Okamura, and G. D. Hager, "Vision-based assistance for ophthalmic micro-surgery," in *Proc. Med. Img. Comput. Comput. Assist. Interven.*, 2004, pp. 49–57.

[25] H. C. Lin, K. Mills, P. Kazanzides, G. D. Hager, P. Marayong, A. M. Okamura, and R. Karam, "Portability and applicability of virtual fixtures across medical and manufacturing tasks," in *Proc. IEEE Int. Conf. Robot. Autom.*, May 2006, pp. 225–231.

[26] R. A. MacLachlan and C. N. Riviere, "High-speed microscale optical tracking using digital frequency-domain multiplexing," *IEEE Trans. Instrum. Meas.*, vol. 58, no. 6, pp. 1991–2001, Jun. 2009.

[27] K. C. Veluvolu, W. T. Latt, and W. T. Ang, "Double adaptive bandlimited multiple Fourier linear combiner for real-time estimation/filtering of physiological tremor," *Biomed. Sig. Proces. Con.*, vol. 5, no. 1, pp. 37–44, 2010.

[28] S. Hutchinson, G. D. Hager, and P. I. Corke, "A tutorial on visual servo control," *IEEE Trans. Robot. Autom.*, vol. 12, no. 5, pp. 651–670, Oct. 1996.

[29] X. D. Chen, J. H. Yong, G. Wang, J. C. Paul, and G. Xu, "Computing the minimum distance between a point and a nurbs curve," *Comput.-Aided Design*, vol. 40, no. 10–11, pp. 1051–1054, 2008.
[30] R. Richa, P. Poignet, and Chao Liu, "Three-dimensional motion tracking for beating heart surgery using a thin-plate spline deformable model," *Intl. J. Robot. Res.*, vol. 29, no. 2–3, pp. 218–230, 2010.
[31] H. Hirschmuller, "Stereo processing by semiglobal matching and mutual information," *IEEE Trans. Pattern Anal. Mach. Intell.*, vol. 30, no. 2, pp. 328–341, Feb. 2008.
[32] P. J. Besl and N. D. McKay, "A method for registration of 3-D shapes," *IEEE Trans. Pattern Anal. Mach. Intell.*, vol. 14, no. 2, pp. 239–256, Feb. 1992.

Brian C. Becker (M'05) received the B.S. degree in computer engineering from the University of Central Florida, Orlando, FL, USA, in 2007 and the M.S. and Ph.D. degrees in robotics from Carnegie Mellon University, Pittsburgh, PA, USA, in 2010 and 2012, respectively.

He is currently a Senior Robotics Engineer with the National Robotics Engineering Consortium, Carnegie Mellon University. He currently specializes in computer vision, control systems, and microsurgical instruments.

Robert A. MacLachlan (M'01) received the B.S. degree in applied mathematics from Carnegie Mellon University, Pittsburgh, PA, USA, in 1987.

He has been a Research Software Developer and an Engineer with Carnegie-Mellon University since 1983 and has been involved in electronic design since 1993. In 1999, he joined the Robotics Institute at Carnegie Mellon, where he has designed and developed sensor and control hardware and software for mobile robots and currently develops intelligent medical instruments with the Surgical Mechatronics Laboratory. His research interests include medical robotics, sensor design, signal processing, and control systems, with particular emphasis on exploiting the combination of sensitive measurements and effective data interpretation algorithms in order to enable the construction of novel mechatronic systems that solve real-world problems.

Louis A. Lobes, Jr. received the M.D. degree from Cornell University Medical College, Pittsburgh, PA, USA, in 1970.

He has been a Clinical Associate Professor of Ophthalmology with the University of Pittsburgh School of Medicine since 1984, with clinical concentration in vitreoretinal surgery, macular degeneration, and diabetic retinopathy. He has been a Co-investigator in the following National Institutes of Health-funded studies: Endophthalmitis Vitrectomy Study, Age-Related Eye Disease Study, and Submacular Surgical Trial and Comparison of Age-related Macular Degeneration Treatments Trial. His main current research interest includes the Micron robotics project.

Dr. Lobes is a member of the Retina Society, the Macula Society, and the American Academy of Ophthalmology.

Gregory D. Hager (F'06) received the Ph.D. degree in computer science from the University of Pennsylvania, Philadelphia, PA, USA, in 1988.

He is currently a Professor and the Chair of Computer Science with Johns Hopkins University, Baltimore, MD, USA, and the Deputy Director of the National Science Foundation Engineering Research Center for Computer Integrated Surgical Systems and Technology. His current research interests include time-series analysis of image data, image-guided robotics, medical applications of image analysis and robotics, and human–computer interaction. He has authored or co-authored more than 220 peer-reviewed research articles and books in the area of robotics and computer vision.

Cameron N. Riviere (S'94–M'96–SM'10) received the B.S. degrees in aerospace engineering and ocean engineering from the Virginia Polytechnic Institute and State University, Blacksburg, VA, USA, in 1989 and the Ph.D. degree in mechanical engineering from The Johns Hopkins University, Baltimore, MD, USA, in 1995.

Since 1995, he has been with the Robotics Institute, Carnegie Mellon University, Pittsburgh, PA, USA, where he is currently an Associate Research Professor and the Director of the Surgical Mechatronics Laboratory. His research interests include medical robotics, control systems, signal processing, learning algorithms, and human–machine interfaces for biomedical applications, including surgery and rehabilitation.

Dr. Riviere is an Associate Editor on the Conference Editorial Boards of the IEEE Robotics and Automation Society and the Engineering in Medicine and Biology Society, and he was one of the Guest Editors of the special issue on medical robotics in the *Proceedings of the IEEE* in 2006.